PROCEEDINGS, 41st Workshop on Geothermal Reservoir Engineering
Stanford University, Stanford, California, February 22-24, 2016
SGP-TR-209

Development of a Novel Stress Sensor for In Situ Stress Measurement

Yarom Polsky[1], Ryan J. Daniels[2], Michael J. Lance[1] and Catherine Mattus[1]

[1]Oak Ridge National Laboratory, 1 Bethel Valley Rd, Oak Ridge, TN, 37831

[2]Univ. of Tennessee Knoxville, 444 Greve Hall, 821 Volunteer Blvd, Knoxville, TN 37996

polskyy@ornl.gov

Keywords: In situ, stress, borehole, overcoring, characterization, piezospectroscopy

ABSTRACT

This paper will describe ongoing work to adapt a previously demonstrated method for measuring stress in ceramics to develop a borehole deployed in situ stress sensor. The method involves the use of a cementitious material that exhibits a strong piezo-spectroscopic stress response as a downhole stress gauge. A description of the conceptual approach will be provided along with preliminary analysis and proof-of-concept laboratory results.

1. INTRODUCTION

A number of approaches for measuring the in situ stress state of rock near boreholes have been developed over the years. These include displacement gauges in combination with overcoring, fracture sleeves, and hydraulic fracturing methods in combination with "visual" methods, such as imprinting of deformable packers or observation of location of borehole breakouts using imaging tools, to determine stress direction (Fairhurst, 2003, Haimson, 1978). Only mechanical stress measurements incorporating displacement gauges or fracture sleeves are currently able to measure the complete or horizontal stress states. The former involve the measurement of radial or, in some cases, circumferential deformations at different orientations within a borehole following an overcoring operation (Martino, 1997). Measured deformations produced by the stress relieving overcoring are typically related to the in situ stress state based on the Kirsch solution to a circular hole in an infinite elastic medium. Applying this solution to determination of the in situ stress state requires knowledge of the elastic modulus of the rock. Fracture sleeve methods by comparison use diametral displacement measurements to determine the onset of failure stresses produced by progressive hydrostatic pressurization until fracture occurs. The tool is effectively an instrumented bladder that is deployed within the borehole. This technique is only applicable when the ratio of maximum to minimum horizontal stress is in the range of 1.5 – 2 (Charsley, 2003). While the mechanical methods are in principal able to provide comprehensive estimates of stress magnitude and directions, they generally involve laborious and sensitive implementation schemes, involve mechanically complex devices, and are subject to significant measurement inaccuracies if coupling of the displacement gauge to the rock is poor. Overcoring based measurements of in situ stress have historically been limited to depths much less than 1,000 m (Ljunggren, 2003). Hydraulic fracturing methods for determining minimum horizontal stress magnitude and orientation are by comparison simpler to implement and can be more easily performed at greater depths, but involve interpretation of pressure time methods and can only be performed if the borehole is aligned with one of the principal stress axes (Haimson 2003).

This paper will describe efforts to develop a stress sensor based on the piezospectroscopic response of α-Al_2O_3 that can potentially be used to measure in situ stress. The material being developed is a castable cement that can be deployed downhole to directly measure changes in the stress environment. Use of a formable material with direct stress sensing capability, as opposed to a mechanical device based on displacement measurement, can potentially simplify deployment complexity, sensitivity and reliability. This material is also being developed for use as a sensor for direct measurement of behind casing cement stress. A brief overview of the behavior of the material and method by which its stress condition can be measured will first be provided. An envisioned method for deploying it downhole to measure in situ stress will then be described. The remainder of the paper will present the progress that has been made towards developing a material composition that is suitable for use as a stress sensor along with preliminary experimental results.

2. PIEZOSPECTROSCOPIC STRESS MEASUREMENT

It has previously been proven that photo-stimulated luminescence spectroscopy of α-Al_2O_3 can be used as a stress sensor in cementitious materials (Asmus, 2002). This method has also been successfully used to measure hydrostatic stress in diamond anvil cells for more than 50 years. Measurement of the material condition requires stimulation using of the α-Al_2O_3 with green or blue laser light followed by measurement of its spectroscopic response. α-Al_2O_3 that naturally contains trace amounts of Cr^{3+} exhibits two red lines or R-lines which occur at ~693 nm. Incident light is absorbed into the blue and green absorption bands, non-radiatively de-excites down to the two energy levels corresponding to the R-lines (14430 and 14400 cm^{-1}) and then down to the ground state producing the characteristic luminescence. If the unit cell of Al_2O_3 is distorted, then the energy levels of Cr^{3+} will shift slightly in response to the change in the crystal field. Therefore, a strain will cause the R-lines to shift and this shift is linear up to a few GPa. An example peak shift with stress is displayed in Figure 1. Since both the excitation and luminescent light occurs in the visible region of the electromagnetic spectrum, standard fiber optic probes can be used to induce and collect the spectra. A single stress measurement can be collected in less than 1 second from a region with a diameter as small as ~1 μm which enables mapping of stress across a surface in a reasonable amount of time. Only the hydrostatic stress can be measured in polycrystalline alumina. All data was collected using a Dilor XY800 Raman Microprobe (Horiba, Edison, NJ) with an Ar^+ laser operating at 5145 Å. The incident light was directed on to the sample surface using a standard optical microscope or through a fiber optic probe depending on the experiment.

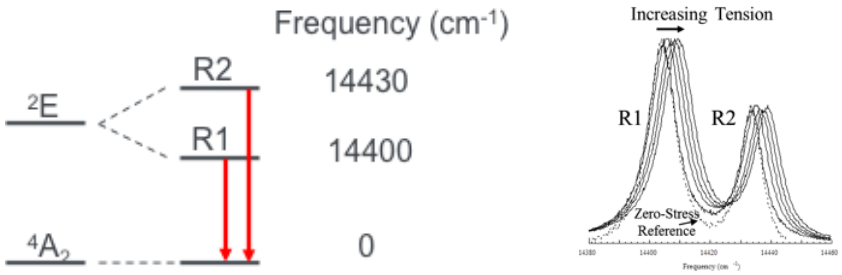

Figure 1: Transition energies and peak shift in alpha alumina with stress change

3. POTENTIAL APPLICATION OF STRESS SENSING MATERIAL FOR IN SITU STRESS MEASUREMENT

The proposed utilization of this material to measure in situ stress involves tailoring a blend of α-Al_2O_3 with cement that can be cast downhole. One implementation of this material for in situ stress measurement involves using the stress sensing material to perform a function similar to a displacement gauge or hard inclusion in a stress relieving overcoring operation. Such operations first involve the drilling of a pilot hole at the bottom of the borehole. The following equations can be used to approximate the stress state near the pilot hole for the general condition where the principal stresses differ in magnitude (Zoback, 1985).

$$\sigma_r = \frac{1}{2}(\sigma_H + \sigma_h)\left(1 - \frac{R^2}{r^2}\right) + \frac{1}{2}(\sigma_H - \sigma_h)\left(1 - 4\frac{R^2}{r^2} + 3\frac{R^4}{r^4}\right)\cos(2\theta) + \frac{\Delta P R^2}{r^2} \quad (1)$$

$$\sigma_\theta = \frac{1}{2}(\sigma_H + \sigma_h)\left(1 + \frac{R^2}{r^2}\right) + \frac{1}{2}(\sigma_H - \sigma_h)\left(1 + 3\frac{R^4}{r^4}\right)\cos(2\theta) - \frac{\Delta P R^2}{r^2} \quad (2)$$

$$\tau_{r\theta} = -\frac{1}{2}(\sigma_H + \sigma_h)\left(1 + 2\frac{R^2}{r^2} - 3\frac{R^4}{r^4}\right)\sin(2\theta) \quad (3)$$

where σ_r is the radial stress, σ_θ is the circumferential stress, $\tau_{r\theta}$ is the shear stress, σ_H is the maximum horizontal principal stress, σ_h is the minimum horizontal principal stress, R is the borehole radius, r is the distance from the center of the borehole, θ is measured from the direction of σ_H, and ΔP is the difference between borehole fluid pressure and formation pressure.

The hydrostatic stress in this condition is obtained by direct summation of equations (1) and (2) and the vertical stress, σ_v, can then by shown to equal:

$$\sigma_{hyd} = \frac{1}{3}\left[\sigma_H + \sigma_h - 2(\sigma_H - \sigma_h)\frac{R^2}{r^2}\cos(2\theta) + \sigma_v\right] \quad (4)$$

When the cement is in a fluid state, it will apply a pressure to the borehole wall corresponding to the ΔP terms in equations (2) and (3). The stress state of the cement plug in the borehole will effectively be hydrostatic even after solidification. Removal of the vertical component of pressure will change the stress state in the plug, but the stresses in the horizontal plane should still be roughly equal in magnitude. It is also noted that the shape of the borehole and cement cross section is elliptical when $\sigma_H \neq \sigma_h$.

Following removal of the in situ stress influences by overcoring, the rock core will experience radial and circumferential deformation as it relaxes. In the limiting case where the deformation is not resisted by an elastic inclusion, and the rock mass is treated as an isotropic elastic material, the radial deformations of the pilot borehole face will vary around the circumference based on the following expression

$$u_r = \frac{r}{E}[\sigma_H + \sigma_h + 2(1 - \upsilon^2(\sigma_H - \sigma_h)\cos(2\theta) - \nu\sigma_v] \quad (5)$$

where u_r is the radial deformation and ν is the Poisson ratio of the rock.

In the case where the stress sensing material within the pilot hole acts as a hard inclusion resisting this deformation, stress will be transferred to the inclusion and the stress state within the inclusion will vary sinusoidally around the circumference. The analytical expressions describing this relationship are complicated and not included in this paper (Kasayapanand, 2008).

If this material and technique could be practically implemented, core sample measurements could be performed after removal from the borehole. Measurements would be performed by cross sectioning of the core followed by piezospectrocscopic evaluation of the circumferential variation on the surface of the hard inclusion. A hole would likely have to be drilled in the center of the hard inclusion to create a stress concentration and amplify the stress state within the material. One potential advantage of this method would be the sectioning and evaluation of cross sections from multiple depths to provide depth based mapping of in situ stress variation.

4. MATERIAL DEVELOPMENT

The development of a stress sensing material formulation that is suitable for downhole application is ongoing. The following performance criteria have been established to ensure that the material is of practical use as a stress sensor: 1) the R1 and R2 peak positions in the material for a uniform stress state should be as consistent as possible within the α-Al_2O_3 and cement mixture in order to

accurately measure stress variation within the sensing material when loaded; 2) the transfer of stress between the cement matrix and α-Al_2O_3 must be adequate to register a response in the α-Al_2O_3 and indicate the stress condition of the composite material; 3) the grout must be slightly expanding while setting in order to maintain contact and measure the response of the borehole wall; and 4) the intensity of the R-lines should be large enough to allow for collection of spectra with a high signal-to-noise ratio in a short amount of time (< 1 minute).

4.1 Peak Measurement Requirements

Spatial consistency of the R line peak values for an equivalent stress state is required if this material is to be used as a stress sensor. For isotropic polycrystalline α-Al_2O_3 the shift in wavenumber can be related to the hydrostatic stress using the expression

$$\Delta\nu = \Pi_{ii}\sigma_h \tag{6}$$

where $\Delta\nu$ is the wavenumber change and Π_{ii} is the piezospectroscopic (PS) coefficient, usually given in units of cm^{-1}/GPa. For reference, the PS coefficient of polycrystalline alumina has been previously determined to be 2.46 cm^{-1}/GPa for the R1 line and 2.50 cm^{-1}/GPa for the R2 line in tension and compression loading tests (Ma, 1993). More recent work has measured the PS coefficient for alumina-epoxy nanocomposites to be between 3.16 cm^{-1}/GPa and 5.63 cm^{-1}/GPa for the R1 line and between 2.6 cm^{-1}/GPa and 5.08 cm^{-1}/GPa for the R2 line when the volume fraction of alumina varies between 5% and 38% (Freihofer, 2014).

These values are presented to illustrate representative ranges of PS coefficients and define practical stress resolution considerations based on the spectroscopic measurement resolution. The target spectral resolution for the project is 0.01 cm^{-1} at 1443 cm^{-1} which corresponds to 1.3 MPa hydrostatic stress for a PS coefficient of 7.62 cm^{-1}/GPa (the PS coefficient for the R2-line of polycrystalline alumina). It is therefore necessary that the signal variability of the alumina powders used to make the stress sensing cement be less than or close to the spectral resolution metric in order to meet stress resolution goals. A number of commercially available alumina powders with different mean particle diameters were obtained and the peak positions at multiple locations in the powders were measured in an unstressed state to assess peak position variability. The results for a measurement spot diameter of 1 µm and 1 mm at 50 mW output laser power are presented in Tables 1 and 2 respectively. It can be seen that the standard deviation of the 1 µm spot size measurements are considerably larger than the target resolution. These variations are likely due to residual stresses, crystal anisotropy, chromium content differences or impurities that cause peak position variation at the microscopic level.

The data for the 1 mm spot size measurements in Table 2 exhibits a considerably lower wavenumber standard deviation. It is believed that this occurs because the 1 mm spot size captures a much larger number of particles and, if the particle orientations are random, this will produce a more consistent average behavior for the measurement area. This data indicates that a number of the powders are suitable for use in the stress sensing material development. The intensity of the measured spectral response in terms of counts per second is presented in the last column of the tables. Larger intensity values are preferred because they reduce the measurement time required to compile a statistically representative peak shape that can be numerically fitted to locate the positions of the R-lines. There is clearly significant variation of this parameter for the different powders.

It is noted that some heat treatment of powders was performed to determine if residual stresses could be relieved and standard deviation of peak positions reduced. There appears to be some improvement in response consistency but more experiments will have to be conducted to compile a statistically relevant conclusion. It is also observed that the intensity of signal progressively increased as the heat treat temperature approached the sintering temperature of 1400°C. A more in depth investigation that also evaluates chromium concentration in the powders will be considered in future work.

Table 1: Standard deviation and intensities of commercially available alumina powders for 10 µm spot size

Powder Description	Particle Size (um)	Spot Size	STD (cm^-1)	Peak Width (cm^-1)	Intensity (counts/s)
Alcoa A2 Unfired	150	10 um	0.0416	9.7270	27212.90
Inframat 200 nm @ 1200°C	0.2	10 um	0.0528	9.4101	45291.20
Inframat 200 nm @ 1400°C	0.2	10 um	0.0574	9.4329	29933.80
Alcoa A2 fired @ 1400°C	150	10 um	0.0911	9.8466	39840.60
Inframat 35 um	35	10 um	0.0930	9.4645	744.30
Type DX 0.3 um	0.3	10 um	0.0965	9.0934	185.13
Inframat 20 um	20	10 um	0.0977	9.5480	4733.30
Inframat 200 nm @ 800°C	0.2	10 um	0.1008	10.1625	4046.38
Type N 0.3 um	0.3	10 um	0.1025	9.3237	122.29
Inframat 200 nm	0.2	10 um	0.1348	12.6365	8336.12
SigAld 10um	10	10 um	0.1434	10.3200	13770.60
Inframat 12 um	12	10 um	0.1501	11.4908	3073.11
Type DX 1 um	1	10 um	0.1543	9.5016	993.38
Inframat 150 nm	0.15	10 um	0.1547	12.9824	9759.59
Inframat 15 um	15	10 um	0.1600	10.4740	1052.95
US Research Nanomaterials 80 nm	0.08	10 um	0.2062		
Inframat 5 um	5	10 um	0.2072	12.6365	4707.27
Inframat 25 um	25	10 um	0.2654	9.9683	1508.66
Inframat 10 um	10	10 um	0.3162	11.7383	5864.28
Inframat 200 nm @ 600°C	0.2	10 um	0.3560	11.4219	6339.77
Inframat_1 to 1_4 mm		10 um	0.4203	12.8563	4452.89
Inframat 200 nm @ 1000°C	0.2	10 um	0.5726	10.2499	3069.41
Inframat 3 um	3	10 um	0.7222	12.9111	5015.05
Alfa Aesar 1um	1	10 um	0.8741	10.5240	2175.00

Table 2: Standard deviation and intensities of commercially available alumina powders for 1 mm spot size

Powder Description	Particle Size (um)	Spot Diameter	STD (cm^-1)	Peak Width (cm^-1)	Intensity (counts/s)
Sigma Aldrich 10 um	10	1mm	0.0055	10.2788	2852.63
Inframat 200 nm @ 1000°C	0.2	1mm	0.0124	9.7918	1151.45
Type N 0.3 um	0.3	1mm	0.0127	9.4725	102.43
Inframat 35 um	35	1mm	0.0130	11.6449	263.16
Inframat 200 nm @ 1400°C	0.2	1mm	0.0173	9.2901	12329.90
Inframat 200 nm @ 600°C	0.2	1mm	0.0178	10.5327	1046.06
Inframat 25 um	25	1mm	0.0182	9.9849	654.75
Inframat 200 nm @ 800°C	0.2	1mm	0.0198	9.9146	1160.60
Inframat 15 um	15	1mm	0.0252	10.1887	185.54
Inframat 40 nm	0.04	1mm	0.0322	12.5234	1641.16
Alfa Aesar 1 um	1	1mm	0.0329	10.2526	672.90
Inframat 200 nm @ 1200°C	0.2	1mm	0.0370	10.2630	1353.84
Inframat 10 um	10	1mm	0.0410	12.0871	1538.6399
Inframat 12 um	12	1mm	0.0421	11.0832	624.99
Inframat 20 um	20	1mm	0.0524	10.1162	723.68
Research Nanomaterials 80nm	0.08	1mm	0.0530	11.1269	12146.36
Inframat 200 nm Control	0.2	1mm	0.0542	11.7894	758.22
Inframat 3 um	3	1mm	0.0664	12.0871	745.35
Type DX 0.3 um	0.3	1mm	0.1496	9.4013	110.12
Type DX 1 um	1	1mm	0.1601	9.5419	215.09
Inframat 5 um	5	1mm	0.1648	12.2630	874.08
Inframat 100 nm	0.1	1mm	0.1921	12.9499	653.57

4.2 Stress Sensing Cement Preparation

Test specimens were initially prepared using the following components with weight fractions summarized in Table 3:

- Ordinary Portland cement (OPC) type I/II from Lafarge (Joppa plant),
- An expansive mineral additive, KOMPONENT from CTS Cement Manufacturing Corp.,
- A high-range water-reducing admixture, MasterGlenium 7700, from BASF Admixtures Systems
- A2 α-Al_2O_3 from Alcoa

To meet the third performance criterion defined at the beginning of this section, an expansive mineral additive was added to the OPC at the level of 15% to counteract the natural shrinkage of the specimen during curing. The dry blend components − OPC, Komponent and alumina − were weighed and mixed in a rotary mixer (30 rpm). The grout preparation was made by first mixing the water and water reducer followed by addition of increasing amounts of dry blend and mixing well by hand after each addition. The piezospectroscopic response of the samples was then measured at different locations but found to be highly variable. Microscopic evaluation of the samples revealed that distribution of the alumina was found to be highly inconsistent due to clumping of the alumina particles.

Table 3: Grout composition for initial specimen blend

	Wt (g)	Wt% of dry blend weight	Wt% of total weight
Type I/II OPC	382.5	54.6	43.5
Komponent	67.5	9.6	7.7
Alumina A2	250	35.7	28.4
Water	175	–	19.9
Glenium 7700	5.3	–	0.6
Dry blend	700	100.0	79.5
Cement paste	880.3	–	100.0
Water/Cement		–	40 %
Water/Solid			26 %
Alumina BWOC (by weight of cement)		55.60%	

New mixing equipment was procured and a new preparation procedure was followed to address the deficiencies found in the initial samples. The new procedures and cement formulation were based on conventional oilfield practice. Subsequent test specimens were prepared using the following components with varying weight fractions of alumina:

- API class H (HSR) cement from Lafarge (Joppa plant),
- An expansive mineral additive, KOMPONENT from CTS Cement Manufacturing Corp.,
- A high-range water-reducing admixture, MasterGlenium 7700, from BASF Admixtures Systems
- α-Al_2O_3 nanopowder from US Research Materials with a particle size of 80 nm

The component weight fractions for a high alumina blend is summarized in Table 4.

Table 4: Grout composition for second specimen blend

	Wt (g)	Wt% of dry blend weight	Wt% of total grout weight
Type H oilwell cement	382.29	54.7	42.1
Komponent	65.93	9.4	7.3
Alumina 80nm	250.12	35.8	27.6
Water	202.37		22.3
Glenium 7700	6.45		0.7
Dry blend	698.34	100.0	77.0
Cement paste	907.16		100.0
Water/Cement			47 %
Water/Solid			30 %
Alumina BWOC (by weight of cement)		55.80%	

The dry blend components − class H cement, Komponent and alumina − were weighed and mixed in a more efficient V-blender. The grout preparation was made by first mixing the water and water reducer. The dry blend was added progressively and mixed by hand with the help of a spindle drink mixer. The high shear mixer was able to fluidify the grout well before the next dry blend addition. At the end of the dry blend addition, the grout was mixed for about 30-45 seconds at high speed in the mixer.

Length and weight changes for the grout prepared with the A2 alumina were monitored on prismatic specimens 25 mm × 25 mm × 250 mm. following ASTM C806. For curing, the specimens were kept in a plastic bag containing a wet piece of tissue to prevent drying. Measurements for samples with 2%, 5% and 10% α-Al_2O_3 by weight fraction are displayed in Figure 2. Results confirmed that a length expansion was obtained for all alumina concentrations up to 42 days of curing.

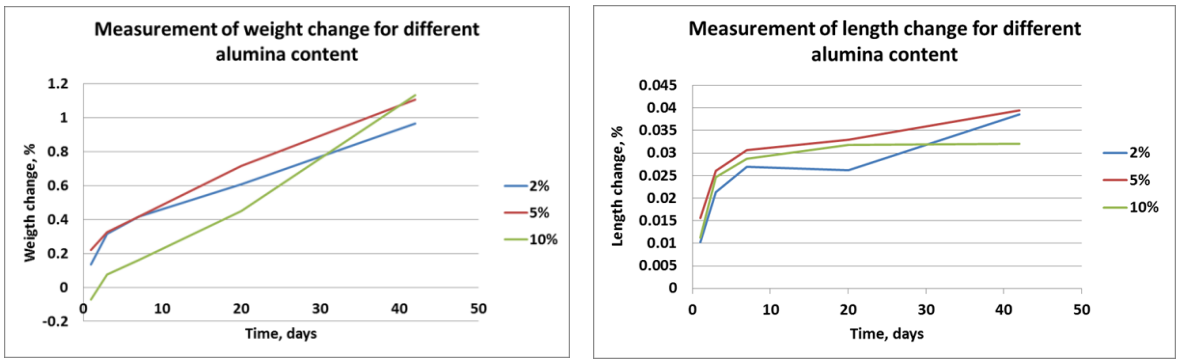

Figure 2: Weight and length evolution of 2%, 5% and 10% alumina dry weight fraction samples vs. time

4.3 Piezospectroscopic response characterization of samples

Piezospectroscopic response of the cement mixtures was measured at different locations of the cured test coupons. Preliminary measurements indicated that the wavenumber standard deviation was more than an order of magnitude larger than desired for the target stress resolution. It was suspected that this variation might be due to localized heating differences produced by the laser stimulation. These temperature differences are likely due to local variations in the alumina concentration. A heterogeneous alumina distribution combined with a lower thermal conductivity of the cement compared to alumina (~1.8 W/m/K compared to 18 W/m/K) will affect the heat conduction rate away from the irradiated surface. This suspicion was confirmed by performing a series of measurements along a 10 mm line with a 1 mm spot diameter on the cement sample surface at different laser power levels. Figure 3 shows a significant increase in the wavenumber standard deviation with increasing laser power for both wet and dry cement samples made from the 80 nm α-Al_2O_3 powders. The standard deviation of the peak position for laser power levels below 100 mW is nearly equal to that of the powder levels before mixing.

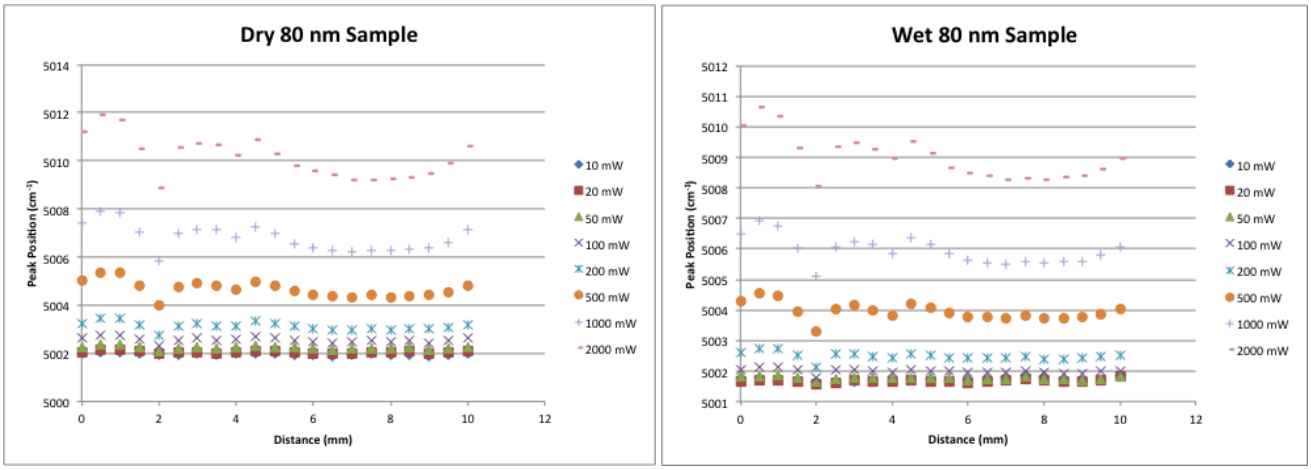

Figure 3: R2 peak position measured for 1 mm spot size at different locations along a 10 mm line segment on dry (left) and wet (right) API class H cement sample with 33.3% 80 nm alumina solid volume fraction for different laser power magnitudes

5. TESTING OF SAMPLES UNDER LOAD

Uniaxial compression tests of stress sensing cement samples were performed to characterize the piezospectroscopic response as a function of loading. Results are shown for two representative samples in Figure 4. The loading curves for both samples indicate that the transfer of load from the cement to the alumina did not occur until the yield point of the cement was reached. Both samples displayed softening behavior between 30 MPa and 40 MPa as evidenced by drops in the load cell value when displacement was paused to make measurements. The unloading curves indicate improved transfer of the load between the cement and the alumina at the lower stress levels with the samples on the far left and far right exhibiting a linear response down to approximately 6 MPa and 13 MPa respectively. Additional investigation will have to be performed to understand the mechanism of load transfer, but it has been previously shown that the presence of voids, inclusions and defects such as microcracks contribute to load transfer in alumina-epoxy nanocomposites (Fugon-Dessources, 2012). These results are nonetheless encouraging and provide preliminary indication that the alumina response can be used to provide a good measure of the stress response of the bulk material.

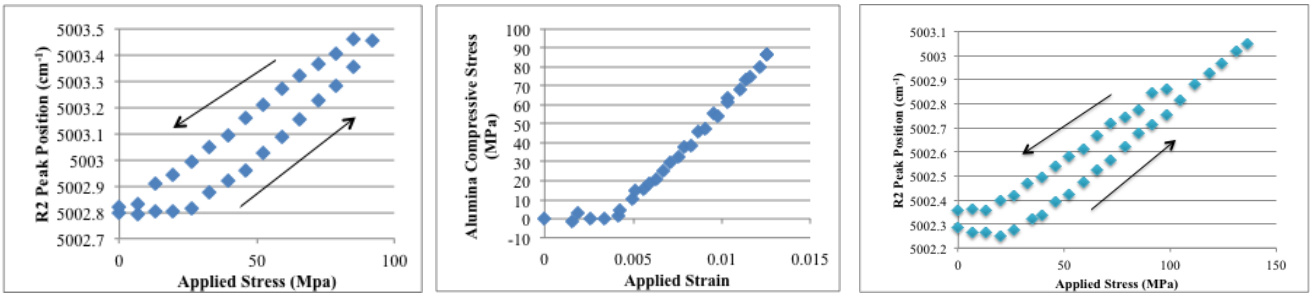

Figure 4: Peak shift versus applied load for two API class H cement samples with 33.3% 80 nm Alumina solid volume fraction. Arrows indicate loading and unloading directions. Middle plot shows alumina stress versus strain during loading for sample test on left.

A laboratory test setup was developed to determine if the stress sensing material could be used as a borehole stress gauge. The test simulates the elliptical deformation of the borehole (or relaxation from an initial elliptical shape) that would be expected with $\sigma_H \neq \sigma_h$. A stainless steel pressure vessel (see Figure 5) was used to perform the experiment. The stress sensing cement sample was cast in the pressure cell while it was loaded on one face with a hydraulic press pressure of 24.5 MPa, which corresponds to approximately 17.5 MPa on the face of the block (test setup shown in Figure 6). A Nitrogen gas bottle was used to pressurize the interior of the vessel to 14.5 MPa while curing in order to simulate the hydrostatic pressure that might exist in a borehole. Following cure, a hole was drilled in the sample to produce a stress concentration in the cement. Piezospectroscopic measurements were then made at the points of expected minimum and maximum stress as the load was removed to simulate the stress relief that would be experienced in an overcoring operation. It is noted that the sample cast in the cell was based on the mixture described in Table 3. As stated in section 4.2, this material did not exhibit a consistent piezospectroscopic behavior due to alumina clumping. To account for this inconsistency, measurements at successive load levels were performed with the measurement probe fixed on the same point on the sample in order to evaluate the relative response of the stress sensing material.

Measurement point locations on the sample with respect to load orientation are shown in Figure 7. The piezospectroscopic response for each of the four points was measured at hydraulic press pressures of 0 MPa, 7 MPa, 14 MPa, 21 MPa and 24.5 MPa. Three separate load cycles were measured for each point. The R2 peak position versus hydraulic press pressure for the four points are shown in Figure 8. The expected trend in this progressive loading scenario is decreasing peak position, corresponding to an increase in compressive stress, for points 1 and 3 (which are perpendicular to the load path) and increasing peak position, corresponding to an increase in tensile stress,

for points 2 and 4. Furthermore, the magnitude of the stress change at successive loads for points 1 and 3 should be three times larger than that for points 2 and 4 because they are located at the positions of maximum stress concentration. While the stress change trend appears to be present for points 1 and 3, it is less consistent for point 2 and is the opposite of what is expected for point 4. The magnitudes of the change in peak position are also considerably larger than expected when compared to the estimated stress levels that should be imparted to the cement through the pressure cell. For reference, the maximum deformation of the inner wall of the pressure cell was estimated to be on the order of 10 μm based on finite element analysis and maximum hydrostatic stress change was estimated to be on the order of 2 MPa, as opposed to the measured value of 7 MPa, for points 1 and 3 assuming an elastic modulus of 20 GPa. Also, it is known that temperature-induced peak shift on the order of 0.14 cm^{-1}/K occurs so corrections should be made if the temperature varies during the experiment (Ma, 1993). Temperature was not measured during this experiment but will be monitored in the future. This experiment was also performed before the effect of laser heating on sample response was known. Measurements were made using 500 mW laser power which was subsequently shown to amplify response differences related to material non-uniformities as described in section 4. The results of this test are therefore considered inconclusive and will have to be repeated.

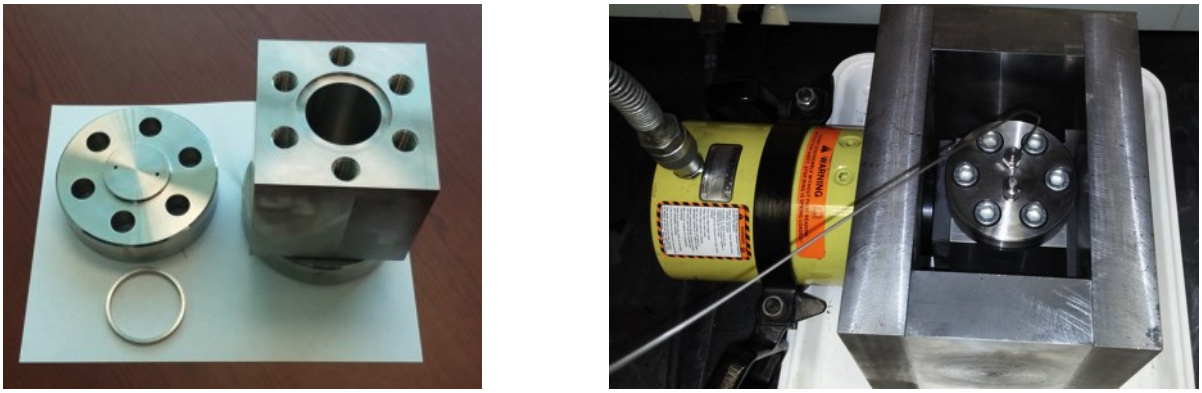

Figure 5: Pressure cell disassembled (left) and in hydraulic press under load during curing (right)

Figure 6: Measurements being performed after one week of curing (left) and sample with 19 mm hole drilled in center of core to produce stress concentration (right)

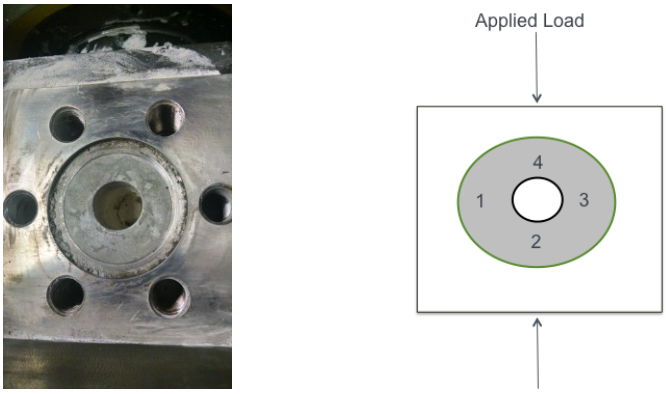

Figure 7: Sample surface (left) and measurement points with respect to applied load (right)

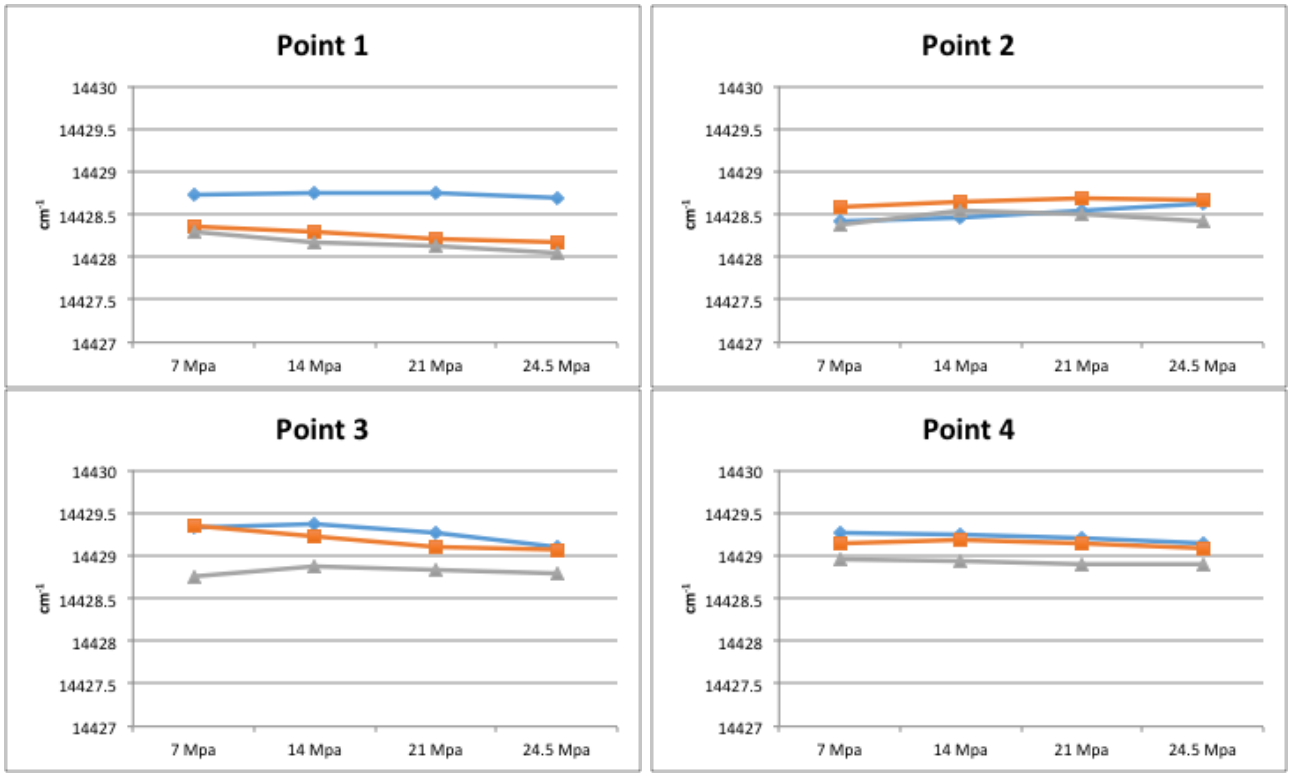

Figure 8: R2 peak position vs hydraulic press pressure at different measurement locations for 38.5% by dry weight Alcoa A2 alumina mixture with Portland cement

5. CONCLUSION

Progress in the development of a stress sensing material for downhole applications has been described in detail including a possible approach for in situ stress measurement based on the conventional overcoring technique. Control of the α-Al_2O_3 behavior in both powder and grout form for use as a stress gauge has proven to be challenging, but systematic improvements in material selection and preparation techniques have shown that a stress indicating grout can be created using both Portland and API class H based cement formulations. The consistency of the piezospectroscopic response of the best performing grout made to date is sufficient for measuring a spatially varying hydrostatic stress response of approximately 6 MPa. Further performance improvements will focus on control of impurities, chromium content, and the use of heat treatment to remove residual stress and increase signal intensity of the alumina. Improved grout preparation procedures will also be developed to better homogenize alumina distribution and mitigate heating variation during laser stimulation of the material.

Pressure cell experiments that simulate the ability of the stress sensing material to measure borehole response in order to infer in situ stress conditions have been inconclusive to date, presumably due to material deficiencies and the need to compensate for ambient temperature variations. The experimental procedure and material formulation will be adapted to compensate for these deficiencies. Specifically, increase of the expansion and modulus of elasticity of the grout during cure will be pursued to better resist the deformation of the borehole wall and increase stress responsiveness. Compensation methods to account for temperature induced R1-line and R2-line peak position shifts will also be incorporated in future experiments.

ACKNOWLEDGEMENTS

Research supported by the Geothermal Technologies Office, Office of Energy Efficiency and Renewable Energy, U.S. Department of Energy under contract DE-AC05-00OR22725, Oak Ridge National Laboratory, managed and operated by UT-Battelle, LLC.

REFERENCES

Asmus and Pezzotti: “Analysis of Microstresses in Cement Paste by Fluorescence Piezospectroscopy,” *Physical Review E*, **66**, (2002).

Charsley, A.D., Martin C.D. and McCreath, D.R.: Sleeve Fracturing Limitations for Measuring In Situ Stress in an Anistropic Stress Environment, *Int. J. of Rock Mech. And Mining Sci.*, **40**, (2003), 127 – 136.

Fairhurst, C.: Stress Estimation in Rock: A Brief History and Review, *Int. J. of Rock Mech. And Mining Sci.*, **40**, Iss. 7-8, (2003), 957 – 973.

Freihofer, G., Schulzgen, A., and Raghavan, S.: Multiscale Mechanics to Determine Nanocomposite Elastic Properties with Piezospectroscopy, *Acta Mat.*, (2014), **81**, 211 – 218.

Fugon-Dessources, D.: Piezospectroscopic Calibration of Alumina-Nanocomposites for the Development of Stress-Sensing Structures, *M.S. Thesis*, university of Central Florida, (2012).

Gladwin, M.T. and Hart, R.: Design Parameters for Borehole Instrumentation, *Pure Appl. Geophys.*, **123**, (1985), 59 – 80.

Haimson, B.C.: The Hydrofractruing Stress Measuring Method and Recent Field Results, *Int. J. of Rock Mech. Min. Sci. & Geomech. Abstr.*, **15**, (1978), pp. 167 - 178.

Haimson, B.C. and Cornet, F.H.: ISRM Suggested Methods for Rock Stress Estimation—Part 3: Hydraulic Fracturing (HF) and/or Hydraulic Testing of Pre-existing Fractures (HTPF), *Int. J. of Rock Mech. And Mining Sci.*, **40**, (2003), 1011 - 1020.

Hudson, J.: Comprehensive Rock Engineering – Principles, Practice & Projects, Vol. 3 Rock Testing and Site Characterization, Ch. 13, Pergammon Press, (1993), 330.

Kasayapanand, N.: Exact Solution of Double Filled Hole in an Infinite Plate, *J. of Mech. Of Mat. And Struc.*, (2008), 101 – 109.

Ljunggren, C, Chang, Y., and Christiansson, R.: An Overview of Rock Stress Measurement Methods, *Int. J. of Rock Mech. And Mining Sci.*, **40**, (2003), 975 - 989.

Ma, Q. and Clarke, D.R.: Stress Measurement in Single-Crystal and Polycrystalline Ceramics Using Their Optical Fluorescence, *J of the Amer. Ceramic Soc.,* **76**, No. 6, (1993), 1433–1440.

Martino, J.B., Thompson, P.M. and Chandler, N.A.:The In Situ Stress Program at AECL's Underground Research Laboratory; 15 Years of Research (1982 – 1997), Report No. 06819-REP-01200-0053 ROO, (1997).

Wong, T.F. and Walsh J.B.: A Theoretical Analysis of Tectonic Stress Relief During Overcoring, *Int. J. of Rock Mech. Min. Sci. & Geomech. Abstr.*, **22**, (1985), pp. 163 - 171.

Zoback, M., Moos, D. and Mastin, L.: Well Bore Breakouts and In Situ Stress, *J. Geophys. Res.*, **90**, B7, (1985), 5523 – 5530.